An Integrated MASS/DIMM Monitor Based on a Low-Noise CCD Detector

A.Guesalaga[*,a,b,c], J.Osborn[d], M.Sarazin[e], B.Neichel[c], S. Perera[d], R.Wilson[d], Peter Wizinowich[e]
[a]Pontificia Universidad Católica de Chile;
[b]Fellow IMéRA Foundation, Aix Marseille Université, France;
[c]Laboratoire d'Astrophysique de Marseille LAM, France;
[d]Durham University, United Kingdom;
[e]European Southern Observatory, Garching, Germany;
[f]W. M. Keck Observatory, USA

ABSTRACT

We propose a novel design for a turbulence profiler. Using a single detector, images of the pupil (scintillation) and stars (image motion) are formed in the detector plane. The instrument is called FASS (Full Aperture Scintillation Sensor), as it uses the full aperture of the telescope. Different processing strategies are evaluated, including spatial segmentation and Fourier analysis. The different approaches are tested via simulation and on-sky data from two telescopes and compared to profiles obtained with the Durham Stereo-SCIDAR monitor. Overall, simulations shows that the method is more accurate that the classical MASS configuration, but it is shown that the photon noise plays an important role in the accuracy of the method, imposing stringent requirements on the pixel size, which must be significantly smaller than the speckle size formed from turbulence close to the ground (Fresnel law for speckle size).
Encouraging results have been obtained for on-sky data and compared to contemporaneous profiles obtained with a Stereo-Scidar technique.

Keywords: Atmospheric turbulence monitors, scintillation, CCD

1. INTRODUCTION

The flexibility offered by CCD detectors and associated hardware and software, the integration of the MASS and DIMM [1-4] seems an obvious choice. The approach we propose is shown below, where the light from the telescope's full aperture is transferred to the detector, generating three images; two for image motion measurements (images of the star) and one for scintillation estimation (images of the pupil). The fact that in this setup the full aperture of the telescope is used, have given the name to this method (FASS: Full Aperture Scintillation Sensor).

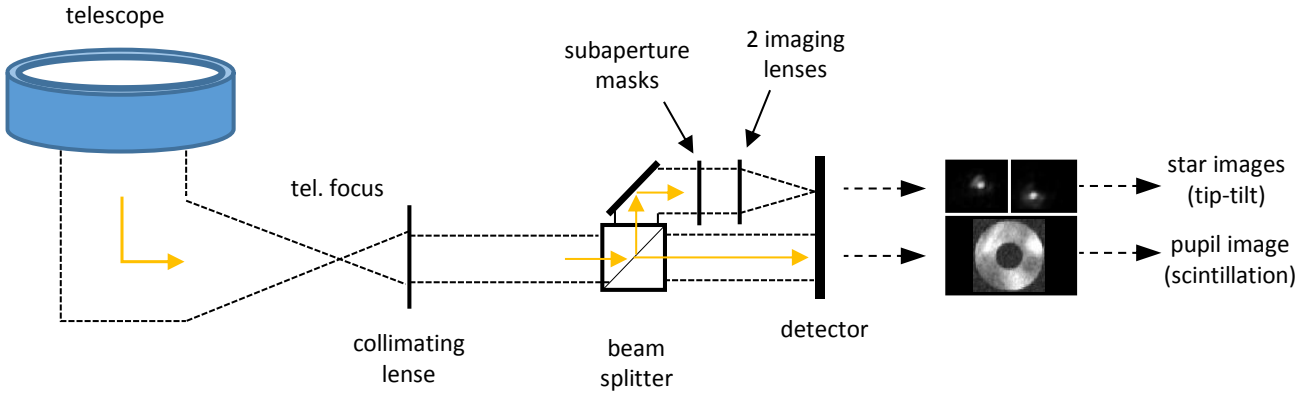

Figure 1. FASS configuration.

[*]aguesala@ing.puc.cl

The longitudinal and transversal image motion variances (S_l and S_t) calculated as described in the DIMM method [3], can be incorporated to the profile of FASS. Next, we focus on the altitude profiling to be estimated from the scintillation generated in the pupil image. It must be noted that DIMM channel is not strictly necessary, i.e. the extra complexity in the optics might not surpass its benefits when compared with a configuration of a single channel (scintillation), working in the generalized configuration (pupil conjugate below the aperture).

2. 2D FOURIER PROCESSING FOR THE PROFILE RECONSTRUCTION

An obvious approach to replace the standard concentric ring configuration of the original MASS method is to extract the speckle size and intensity information from 2D power spectra obtained from images of the full pupil, maximizing the use of the flux received by the telescope.

A mask has been applied to the simulated pupils in order to generate the same diffraction patterns as in the real case. The onsky data has been recorded at the 1.0 m Jacobus Kapteyn Telescope (JKT) on La Palma.

A clear difference exists in the distribution of the power spectra, where smaller speckles populate higher frequencies whereas large speckles caused by high altitude turbulence will tend to concentrate the energy at the centre of the spectrum. This characteristic is used to generate the equivalent of the weighting functions in the new method by splitting the spectrum into concentric frequency rings that span the range of spatial frequencies generated by the speckles.

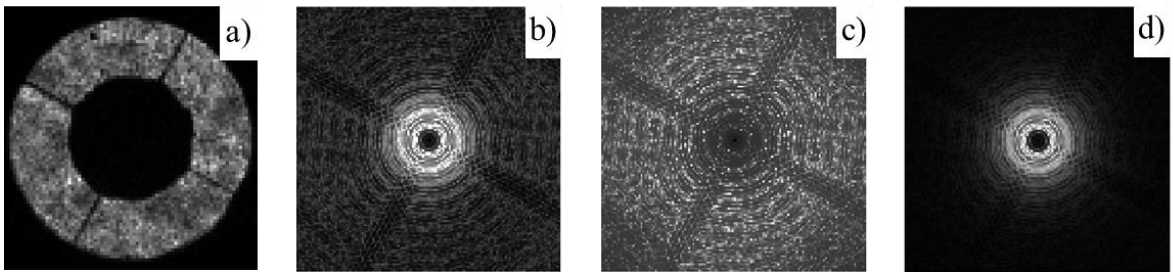

Figure 2. Images from pupil and 2D-power spectra of simulated and real (JKT). a) Pupil image of JKT with central obscuration and spiders; b) average 2D-PSD of JKT sequence c) simulation of a single layer at 500m d) simulation of a single layer at 16,000m.

The next figure shows simulated pupil images of scintillation for the 1 m aperture of the JKT telescope caused by turbulence located at 500m and 10000m respectively and for a seeing of 0.2". A clear distinction among the two cases are obvious, with a speckle size that is proportional to the altitude of the layers that according to the Fresnel law would be $d_s = \sqrt{h \cdot \lambda}$, with h being the altitude of the layer and λ the wavelength of the source (here considered monochromatic at 500nm). So, for the two layers considered: d_s @ 500 = 1.6 cm and d_s @ 10000 = 7.1 cm.

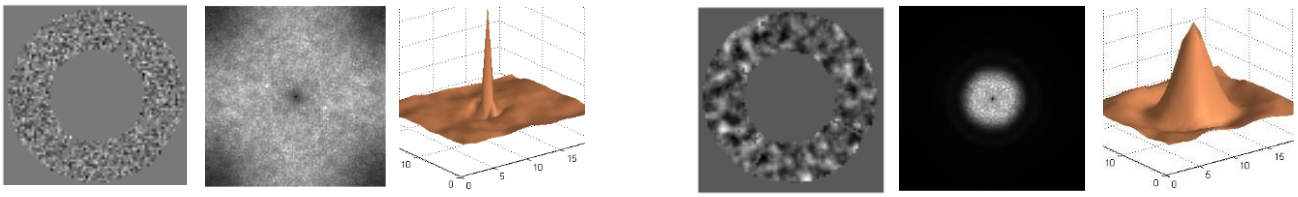

Figure 3. Speckles generated at the pupil; 2D power spectra of speckle images and autocorrelation functions of the pupil images by turbulent layers located at 0.5Km (left trio) and 10Km (right trio).

The pixel size of the camera is 1.4 cm, which a key parameter; essential to separate the noise (read-out or photon noise) from the speckle information. This parameter limits the minimum altitude that the speckles can be reliably detected and in this configuration, speckles generated by turbulence layers below 500 m are not possible to distinguished from the noise, i.e. the pixel size is comparable or even larger the expected speckle average diameter.

The 2D spectra present significantly weaker traces of diffraction rings than in the previous image due to the. Subtraction of the mean value

The weighting functions in this method are 1D frequency curves obtained by integrating the 2D power spectrum in disks of increasing diameter. The three weighting functions in the left plot of the next figure show a very distinctive pattern among them, which is required to solve the inverse problem of estimating the profile (conditioning of the problem). Notice the secondary lobes in each of the curves; they are due to the finite nature of the Fourier transform that generates these diffraction rings. This can be a problem when estimating profiles with highly distributed energy.

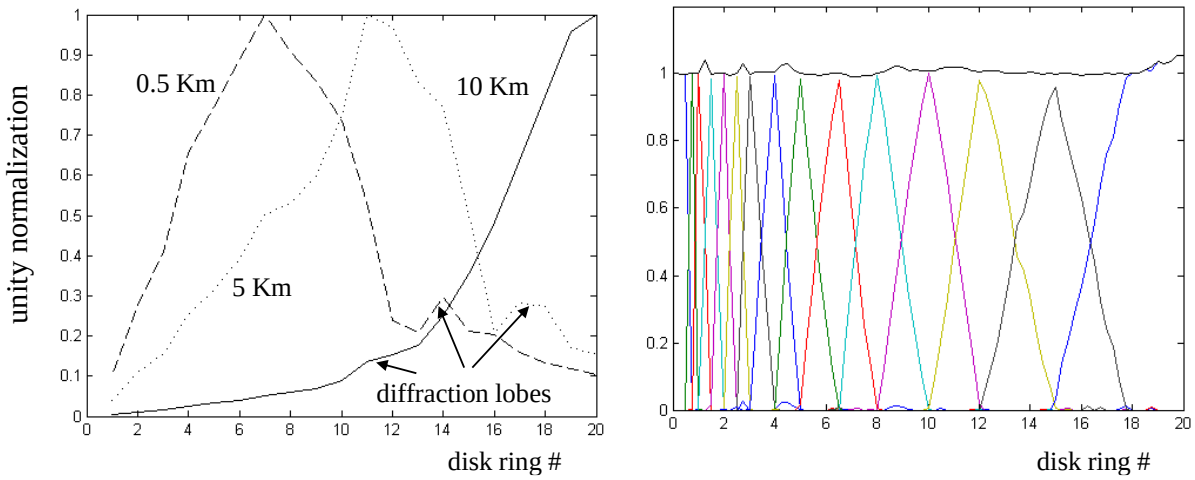

Figure 4. Left: example of 3 frequency curves (weighting functions) for speckles from layers at 0.5Km, 5Km and 10Km. Right: Response of the altitude slabs chosen for turbulences layers. The curve at the top corresponds to the sum of the individual responses.

We have found that for this application (JKT) we can more than double the number of divisions (15) also extending the range of altitudes.

We have defined the following slabs: Z = [0.5 0.75 1.0 1.5 2.0 2.5 3.0 4.0 5.0 6.5 8.0 10.0 12.0 15.0 18.0] (Km)

The response functions for the 15 slabs are substantially better than that of the traditional method in terms of errors, especially at lower slabs, with a much better resolution given by the higher number of slabs (15 against 6 of the classical method).

Sequence of 23.000 frames from Stereo-Scidar. Profiles from SS (left) and FASS (right). The profile of the SS has been re-sampled to match the slabs positions of FASS.

The figure shows a comparison between the FASS method based on Fourier with the profiles results obtained for the Stereo-Scidar technique applied to the JKT. Although the SS approach shows an expected better resolution at lower altitudes (no pixel/speckle size issue) the total energy at lower altitudes are similar ($3.8*10^{-13}$ in the first FASS slab against $3.28*10^{-13}$ in the first 3 slabs of the SS method).

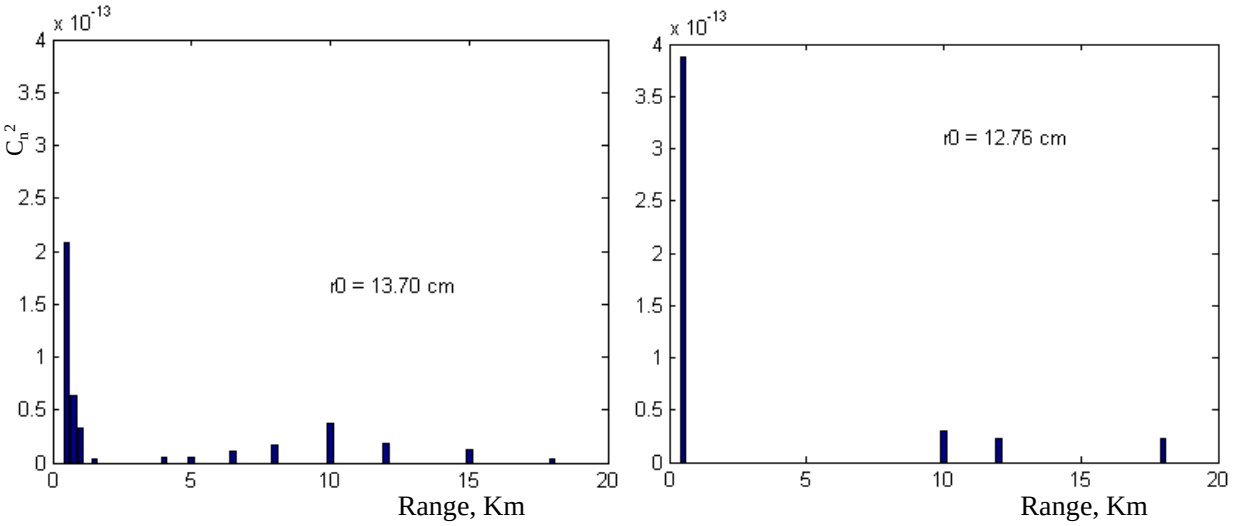

Figure 5. Comparison between the FASS method based on Fourier with the profiles results obtained for the Stereo-Scidar technique applied to the JKT

3. ESTIMATION OF TURBULENCE PROFILE AND SPEED OF LAYERS SPEED USING TEMPORAL CROSS-CORRELATIONS

The pupil speckle images can also be used to estimate the speed of the most significant layers by analyzing the temporal correlations of successive images. This estimation requires that the layers have a minimum speed and direction that guarantees that the correlation peaks are separated along the sequence, so they can be distinguished.

Perhaps as important as getting the speed and direction of the layers, is the fact that their altitude can also be estimated from the width of the correlation peaks. Take the example of the next simulation of three layers located at 0.5, 4 and 12 Km presented in the upper row of the next figure, with a common speed of 20m/s for the 3 layers, but with different wind directions. The first column shows 2D and 3D representation of the correlation functions for $t = 0$. The correlation functions coincide in the map, but for the next 3 frames, the moving layers get separated, giving information about their speeds and directions. Equally important the width of each peak provides information about their location in altitude, as the correlation functions gets broader for larger speckle sizes, i.e. higher altitudes. However, to use this mechanism to estimate layers' altitudes requires that the speckle structure does not change during the first correlations (Taylor's hypothesis). These possible deviations can be alleviated using short exposure times. Vibrations also must be kept to a minimum.

The bottom row shows the result of a sequence of temporal cross correlations from the JKT on-sky data. The sampling frequency is 80Hz approximately. Four peaks are distinguishable with different widths and intensities. The sharper peak corresponds to quasi static speckles located near the ground (e.g. dome seeing or optical aberrations), whereas the other three have been generated by layers at higher altitudes.

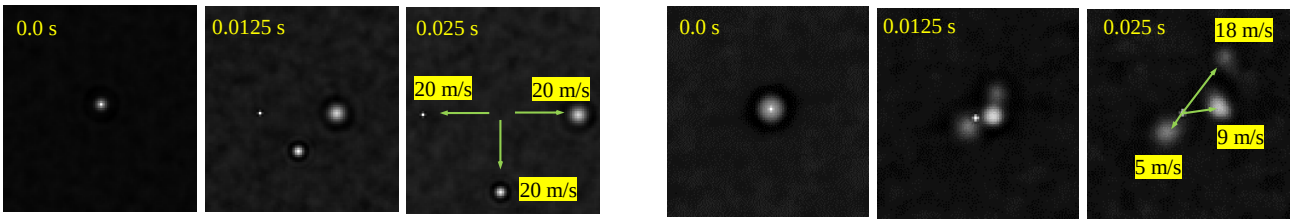

Figure 6. Temporal correlations of speckle images (Left trio: simulated; Right trio: on-sky data). The sharper peaks are from speckles located near the ground, whereas wider ones have been generated by layers at high altitudes

4. SOLUTION FOR SMALL TELESCOPES (1D FOURIER PROCESSING)

One of the main objectives of this study is to evaluate this new approach in small telescopes, i.e. less than 30cm in diameter. This is essential as it would allow the development of a low cost instrument.

Data from a telescope (Celestron C9.25 XLT, 23.5cm diameter) has been used in the following analysis. The speckles size in this case are comparable to the width of the pupil ring. A 2D processing would be impractical as these large speckles would generate an important amount of leakage in the frequency spectra due to the finite nature of the Fourier transform. However, by resampling the image along the ring a longer length of the image data could be possible, were more than one of these large speckle could fit. For example, a ring defined by a radius of r = 10 cm, would generate a sampled perimeter of $2\pi r \approx 60$cm, which can accommodate up to three complete cycles of 10 cm speckles (resulting after propagating a wavefront from a layer at 18Km).

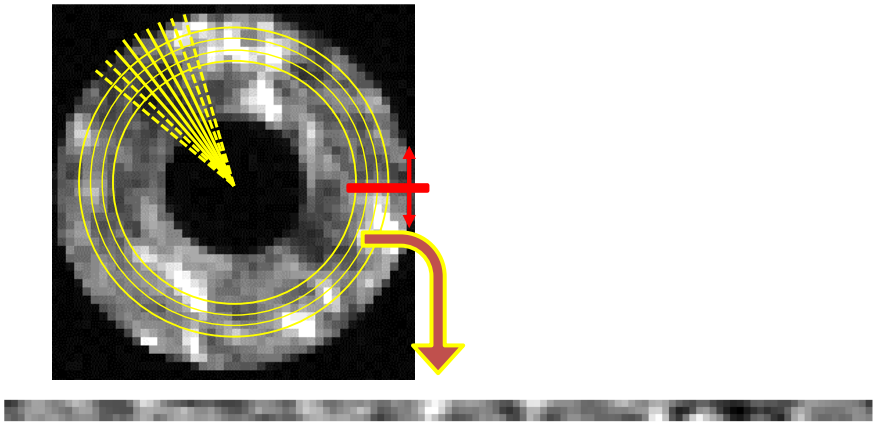

Figure 7. Unravelling the 3 rings via interpolation and polar grid

The lines of the resulting matrix (length 128) are Fourier transformed and later averaged. One of the advantages of such resampling, is that the transformation is circular, so no distortions due to its finite nature are expected.

No significant distortion in the information contained in the image occurs as long as the total thickness of the ring is much smaller than its diameter and for an odd number of lines, the stretching of the outer rings would tend to cancel the effect of the compression of the inner ones. Multiple single line rings covering the full aperture could be used. In this case however, the components of the resulting spectrum would have different values, so a resampling of the spectra into a common frequency range would be necessary.

On the other extreme of the speckles side range, according to Fresnel law, the size of a speckle generated by a layer at 500m, would be around 1.7cm which is more than twice the size of the image pixel (pupil units), so pixel noise (readout or photon) should be possible to be differentiated from the smallest speckle for the layer at 500m.

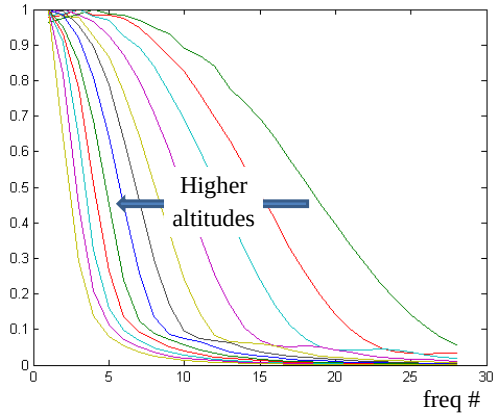

Figure 8. 12 weighting functions. Only the first 28 points suffice to estimate the profile

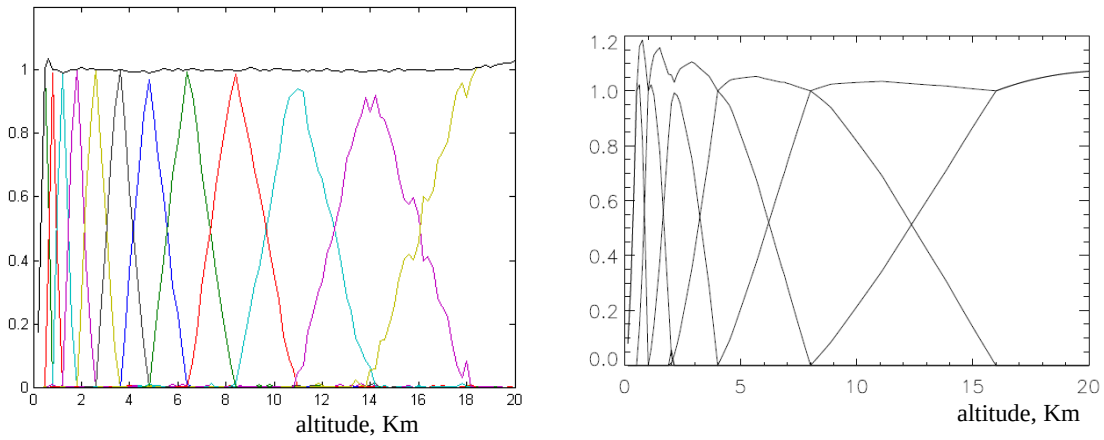

Figure 9. Response of slabs for FASS (left) and MASS (right).

The figure in the extreme left shows the response of the 12 slabs, from 0.5Km to 18Km. They behave extremely well for lower altitudes, however a departure from ideal performance is observed for higher slabs. The rugosity in the response of the higher 3 slabs are not important as it corresponds to a transfer of energy to neighbour slabs (minor errors in altitude estimation). Furthermore, the sum of the total contributions of the slabs are kept close to 1.

5. ON-SKY DATA FROM A SMALL TELESCOPE

Data from the Celestron telescope consists of 59 groups of 5,000 frames each, taken during the nights of the 27th, 28th and 29th of September 2014. The camera used to get the images is an Andor Luca-S EM-CCD, with 10 μm pixels, 4x4 binning (40 μm effective pixel size) and exposure time of 1 msec and frame rate of 150 Hz. The detector was placed conjugate to telescope pupil and no filter was used. The target star is Vega.

The data from pupil images conjugated at the ground are accompanied by profiles obtained with a Stereo Scidar (SS) instrument installed on the 2.5m INT telescope, 10m away from the Celestron telescope. These profiles are approximately contemporaneous for each observation of the Celestron telescope. The SS instrument is conjugated at -2.3Km, so it provides estimations of turbulence at the ground. Unfortunately, no complete comparison with our technique can be made as no reliable estimations at the ground exists for the Celestron telescope (conjugation at 0Km).

The next figure presents 3 cases, representatives of the profiles observed during these three nights. In each plot, the yellow bars correspond to the profiles obtained with FASS. Superimposed are the contemporaneous profiles obtained with Durham's Stereo-Scidar approach.

Notice that except for the first slab (no reliable estimation for FASS), the spectra is similar, except for one simple but very important characteristic: The FASS profiles are shifted towards the right (i.e. higher altitudes). This effect was observed in almost all 59 profiles.

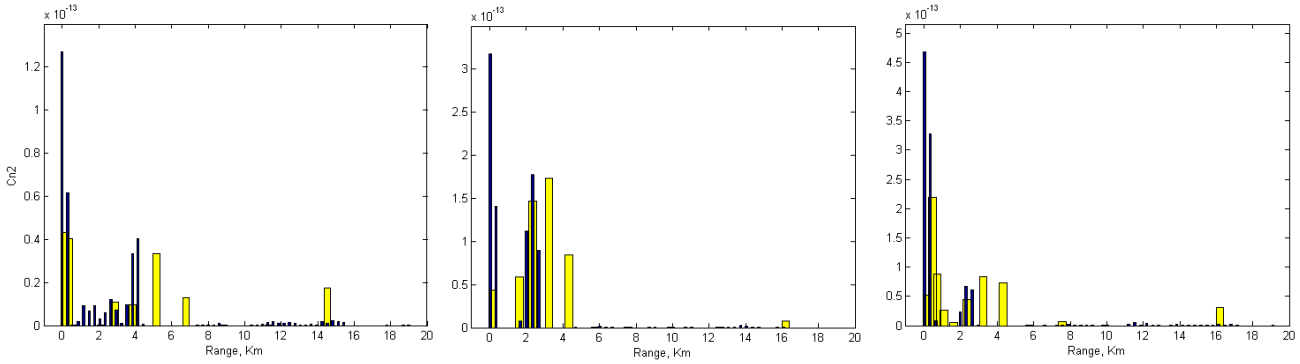

Figure 10. Profiles from the nights of the 27th, 28th and 29th of September 2014. The blue bars are from Durham's SS and the yellow bars correspond to FASS.

The overestimation of the altitudes can be explained by one of the following factors: i) defocus of the image pupil or bad calibration of the pupil size (wrong pixel size); ii) wind or vibration, enlarging the correlation peak during exposure time; iii) Polychromatic light (not considered here).

A secondary effect of this shifting in altitude, is that they also tend to amplify the estimation of upper layers, attenuating the ones near the ground.

6. CONCLUSIONS

Careful definition of specifications for the optics and components are needed. In particular, aspects such as detector integration time, opto-mechanical stability and detailed spectrum modelling of stars and detector are needed for good estimations, especially regarding altitude estimation accuracy.

The size of the pixel is also a crucial parameter and can severely limit the accuracy at low altitudes, as the size of the associated speckles become comparable to the pixel size and hence, to the detector noise spatial distribution.

We think that the generalized method is a must and significant effort should be devoted to design a robust optics to achieve this.

Other pending activities are adapting the method to strong turbulence regimes and the extension of the method to polychromatic light.

REFERENCES

[1] Kornilov V.,Tokovinin A.,Voziakova O.,Zaitsev A.,Shatsky, N.,Potanin S.,Sarazin M., 2003, Proc. SPIE, 4839, 837
[2] Tokovinin A., 2003, J. Opt. Soc. Am. A., 20, 686
[3] Tokovinin A., Kornilov V., 2007, MNRAS, 381, 1179
[4] Kornilov V., Tokovinin A., Shatsky, N.,Voziakova O., Potanin S., Safonov B., MNRAS, **382,** 2007
[5] Shepherd H.W., Osborn J., Wilson R.W., Butterley T., Avila R., Dhillon V.S. and Morris T.J., MNRAS, 2014

ACKNOWLEDGEMENTS

Andrés Guesalaga thanks IMéRA foundation for the support given to develop this work